Title	Volume of high-risk intratumoral subregions at multi-parametric MR imaging predicts overall survival and complements molecular analysis of glioblastoma
Author(s)	Cui, Yi; Ren, Shangjie; Tha, Khin Khin; Wu, Jia; Shirato, Hiroki; Li, Ruijiang
Citation	European Radiology, 27(9), 3583-3592 https://doi.org/10.1007/s00330-017-4751-x
Issue Date	2017-09
Doc URL	http://hdl.handle.net/2115/71443
Rights	This is a post-peer-review, pre-copyedit version of an article published in European radiology. The final authenticated version is available online at: http://dx.doi.org/10.1007/s00330-017-4751-x
Type	article (author version)
File Information	EU_RADIO_CUI.pdf

Manuscript title

Volume of high-risk intratumoral subregions at multi-parametric MR imaging predicts overall survival and complements molecular analysis of glioblastoma

Authors

Yi **Cui**, PhD[1,2], Shangjie **Ren**, PhD[4], Khin Khin **Tha**, MD PhD[2,3], Jia **Wu**, PhD[1], Hiroki **Shirato** MD PhD[2,3], Ruijiang **Li**, PhD[1,2]

Affiliations

1. Department of Radiation Oncology, Stanford University, USA

2. Global Station for Quantum Medical Science and Engineering, Global Institution for Collaborative Research and Education, Hokkaido University, Japan

3. Department of Radiology and Nuclear Medicine, Hokkaido University, Japan

4. School of Electrical Engineering and Automation, Tianjin University, China

Corresponding Author

Yi Cui

Department of Radiation Oncology, Stanford University

1070 Arastradero Rd., Palo Alto, CA 94304, USA

Tel: +1 (650) 724-9383

Email: cuiyi@stanford.edu

Volume of high-risk intratumoral subregions at multi-parametric MR imaging predicts overall survival and complements molecular analysis of glioblastoma

Abstract

Objective

To develop and validate a volume-based, quantitative imaging marker by integrating multi-parametric MR images for predicting glioblastoma survival, and to investigate its relations and synergy with molecular characteristics.

Materials and Methods

We retrospectively analyzed 108 patients with primary glioblastoma. The discovery cohort consisted of 62 patients from the cancer genome atlas (TCGA). Another 46 patients combining 30 from TCGA and 16 internally were used for independent validation. Based on integrated analyses of T1-weighted contrast-enhanced (T1-c) and diffusion-weighted MR images, we identified an intratumoral subregion with both high T1-c and low ADC, and accordingly defined a high-risk volume (HRV). We evaluated its prognostic value and biological significance with genomic data.

Results

On both discovery and validation cohorts, HRV predicted overall survival (OS) (concordance index: 0.642 and 0.653, $P<0.001$ and $P=0.038$, respectively). HRV stratified patients within the proneural molecular subtype (log-rank $P=0.040$, hazard ratio=2.787). We observed different OS among patients depending on their MGMT methylation status and HRV (log-rank $P=0.011$). Patients with unmethylated MGMT and high HRV had significantly shorter survival (median survival: 9.3 versus 18.4 months, log-rank $P=0.002$).

Conclusion

Volume of the high-risk intratumoral subregion identified on multi-parametric MRI predicts glioblastoma survival, and may provide complementary value to genomic information.

Keywords

Multi-parametric MRI, glioblastoma multiforme, high-risk tumor volume, overall survival, radiogenomics

Key Points

1. High-risk volume (HRV) defined on multi-parametric MRI predicted GBM survival.
2. The proneural molecular subtype tended to harbor smaller HRV than other subtypes.
3. Patients with unmethylated MGMT and high HRV had significantly shorter survival.
4. HRV complements genomic information in predicting GBM survival

Introduction

Glioblastoma (GBM) is the most deadly primary brain tumor in adults, with a median survival of 12-15 months despite aggressive treatment [1]. GBM is also a biologically heterogeneous disease, where four subtypes, i.e., the proneural, neural, classical, and mesenchymal subtypes, have been proposed based on molecular characteristics of the tumor [2]. Compared with the molecular approach, imaging provides a unique opportunity to noninvasively interrogate the anatomical and functional properties of the entire tumor. Given the routine use of imaging in GBM management, reliable imaging-based biomarkers would have tremendous value in precision medicine, by stratifying patients to guide individualized therapy.

There has been a significant interest in predicting survival of GBM patients based on multi-parametric magnetic resonance (MR) imaging that incorporates perfusion-weighted imaging [3-5], or diffusion-weighted (DW) imaging [6-12]. Most previous studies defined imaging prognosticators as a single point on the signal intensity histogram, e.g. maximum cerebral blood volume (CBV) [3], minimum apparent diffusion coefficient (ADC) [13], or simple quantiles [6]. On the other hand, volume-based imaging metrics that incorporate both intensity and volumetric information, may be more reliable indicators of tumor burden [14-16]. Furthermore, given the heterogeneous nature of GBM, detecting “high-risk” intratumoral subregions could potentially identify biological relevant, aggressive subclones within a tumor [17], and has therapeutic implications for intensified local therapy to improve survival [18].

Recent preliminary studies have shown promising results for predicting survival of GBM patients based on analysis of intratumoral subregions, using conventional T1-weighted contrast-enhanced (T1-c) and T2-weighted fluid-attenuated inversion recovery (FLAIR) MR images [19; 20]. However, a method to explicitly identify clinically relevant, high-risk tumor volume with robust and meaningful cutoffs has been lacking. Current MR imaging markers based on simple, predefined cutoffs such as median or quantile may not be optimal. In addition, individual cutoffs at the patient level can be sensitive to variations due to differences in image acquisition protocols in different patients [21; 22]. Consequently, these imaging markers are difficult to compare and reproduce across cohorts in multi-center settings, which is a significant hurdle to their clinical translation.

In this study, we hypothesized that the volume of an intratumoral subregion associated with abnormally high signal intensity on T1-weighted contrast-enhanced imaging and abnormally low ADC on DW imaging can quantify the most aggressive disease burden within a tumor, and thus may be a better predictor of prognosis of GBM patients compared with whole-tumor imaging metrics. This is supported by recent studies showing that the tumor-enhancing volume [14] and the volume of low ADC [16] were both prognostic of overall survival in GBM. Instead of using predefined cutoffs for individual patients, we propose a novel method to define robust cutoffs applicable to the entire study population and identify high-risk intratumoral subregions by using a data-driven approach. Further, we evaluated the biological significance of our imaging marker by associating with underlying molecular features. Distinct from most previous radiogenomic studies [23-26], we further investigated whether this imaging marker provides complementary value to the genomic counterparts.

The purpose of this study is two-fold: 1), to develop and validate a new volume-based, quantitative imaging marker by integrating multi-parametric MR images for predicting survival of GBM patients; 2), to investigate the relations and potential synergy between the proposed imaging marker and underlying molecular characteristics of GBM.

Materials and Methods

Study Population

In this institutional-review-board approved study, a total of 108 patients were retrospectively investigated. The inclusion criteria were: 1) pathologically confirmed diagnosis of GBM, 2) availability of preoperative T1-weighted contrast enhanced (T1-c) and diffusion-weighted (DW) images, and 3) availability of information about overall survival. The exclusion criteria were prior surgery and other treatments. The majority of the study cohort, consisting of 92 patients from 1998 to 2011, was retrieved from the Cancer Imaging Archive (TCIA). We initially identified 98 patients from TCIA whereas 6 of them were excluded due to poor image quality (such as motion, metal artifacts, and RF inhomogeneity) as assessed by a neuroradiologist with over 10 years' experience (KKT). Furthermore, we searched patient records from 2004 to 2014 at the local institution using the same inclusion and exclusion criteria and found 31 patients. Fifteen of them were excluded because they did not have echo-planar T2-weighted images with zero diffusion weighting (b = 0 sec/mm^2), leading to 16 additional patients eligible for this study. The median follow-up duration was 10.9 months for the TCIA cohort and 9.6 months for the internal cohort.

We randomly split the TCIA cohort into two portions, where the first one containing approximately two-thirds of the patients (n = 62) was used as a discovery cohort. The remaining portion (n = 30) was combined with internal cohort (n = 16) to form the validation cohort (n = 46). The overall study design and patient cohorts are illustrated in Fig. 1. Clinical and demographic information of the study population is listed in Table 1.

Image Acquisition

Among the 108 patients, the magnetic fields used to acquire the MR images were 1T (n = 1), 1.5T (n = 65), 3T (n = 35), or unknown (n = 7). For the T1-c images, the sequence protocols were spin-echo (n = 77), gradient echo (n = 13), or T1-weighted fluid-attenuated inversion recovery (n = 18). The repetition time and echo time ranged respectively from 6 to 3189 msec, and from 3 to 20 msec. The intra-slice voxel resolution varied from 0.43 mm to 1.02 mm, the slice thickness was between 2.5 mm and 5 mm, and the inter-slice gap was between 0 mm and 2.5 mm. For DW images, the b-values were 1000 sec/mm^2 (n = 103), 1500 sec/mm^2 (n = 5). Echo-planar T2-weighted images with zero diffusion-weighting (b=0 sec/mm^2) were acquired for all the patients (n = 108). The intra-slice voxel resolution, the slice thickness, and the inter-slice gap of the DW images ranged from 0.86 mm to 1.8 mm, 3 mm to 7 mm, and 0 mm to 1 mm, respectively.

Image Processing

For each patient, we co-registered the MR images using the extensively validated software, elastix [27]. Specifically, we used the T1-c image as the reference and rigidly transformed and resliced the echo-planar T2-weighted image with zero diffusion weighting. However, for those cases having noticeable geometric distortion by automatic registration, in-house developed MATLAB software was used instead for manual registration. This process started with visually inspecting the T1-c image and the echo-planar T2-weighted image with zero diffusion weighting to identify slice pairs at the same locations. Then within each slice pair we manually selected landmark points at salient anatomical structures (e.g., ventricles) in both modalities and recorded their 3-dimensional coordinates. Given the corresponding coordinates of the landmarks, we calculated an affine transformation function by least-square estimation to register the echo-planar T2-weighted image with zero diffusion weighting to the T1-c image. Finally, elastix was used to register the DW image to the T2-weighted image with zero diffusion weighting with affine transformation in order to correct for the eddy current distortion and motion effects [28]. The ADC maps were reconstructed from the registered images. Any voxel with negative ADC values due to measurement noise was set to zero and then imputed from its neighborhood.

Image Normalization

Given the non-uniform imaging protocols and parameters of the MR images in the multi-institutional cohort, it is mandatory to normalize the image data acquired under different conditions. To this end, we proposed a novel standardization approach based on kernel density estimation (KDE). KDE is an unsupervised machine learning technique able to estimate the probability density function (PDF) underlying the observed data. It does not assume a parametric form for the PDF to be estimated and therefore particularly suitable for charactering irregular (non-Gaussian) distributions. Specifically, for each T1-c or ADC image, we applied the KDE to estimate the continuous PDF of the intensities for voxels within the entire brain parenchyma. We then normalized the image by dividing each voxel with the mode of this PDF (Fig. 2). The rationale for this approach is that the mode represents the most frequently occurring voxel value in the image, which comes from the normal-appearing white matter that constitutes the majority of brain tissues. For PDF estimation we used the MATLAB code which used the Gaussian kernel and was able to automatically choose the kernel bandwidth based on the "plug-in" KDE algorithm [29]. In order to avoid estimating the background noise, we set the interval on which the density estimate was constructed to be [max/50, max] where max denoted the maximum intensity of the image and used 10^8 meshes to discretize this interval. It should be noted that although some studies reported similar ADC values among scanners when identical image acquisition parameters were used [30-32], the imaging parameters in our study were not consistent. Therefore, in order to minimize the effects of inter-scanner variations, we chose to normalize the ADC maps. ADC normalization was also performed in other studies [33], where relative ADC maps were used to correlate with genetic and cellular GBM features.

High-Risk Volume Identification

The gross tumor volume(GTV), including both the contrast-enhanced area as well as the bounded non-enhancing and necrotic regions, was segmented semi-automatically on T1-c images using MIPAV [34]. This process used the built-in level-set algorithm of MIPAV and entailed the operator moving the cursor around the boundary of the tumor which was then automatically captured. Manual correction was performed in 8 cases where automatic segmentation failed. In order to assess the reproducibility of the segmentation as well as its impact on subsequent analyses, all tumors were independently delineated by two observers

(SJR and YC). Dice and intra-class correlation coefficients were calculated for the two tumor segmentations.

After segmentation, we defined the high-risk volume (HRV) as the volume of the intratumoral subregion with both higher T1-c intensity and lower ADC. In order to obtain robust and meaningful thresholds to identify the HRV, we pooled the tumor voxels of all the patients in the discovery cohort, for the normalized T1-c and ADC images respectively. For each sequence we used the KDE to estimate their pooled PDFs and used the mode values as global cutoffs, hereafter denoted as t_1 and t_2. The rationale for the use of mode is that statistically speaking, it is the most typical value of a certain population: any value above or below this value may be considered abnormally high or low. The HRV of an individual patient was defined as the volume of the tumor satisfying T1-c > t_1 and ADC < t_2. Fig. 2 illustrates the hierarchical flowchart for HRV identification. Once identified, the same thresholds were used to define the HRV for patients in the validation cohort. We examined whether HRV predicted overall survival (OS) in both discovery and validation cohorts. In addition to HRV, we computed the enhancing tumor volume (ETV), which we defined as the volume of the tumor satisfying T1-c > 1. The OS prediction performance of ETV was also evaluated.

Relations between high-risk volume and molecular features

We investigated the associations between the proposed imaging marker (HRV) and four molecular subtypes of GBM, i.e., the proneural, neural, classical, and mesenchymal subtypes, which was obtained for 88 patients in the TCIA cohort from the UCSC Cancer Genomics Browser [35; 36]. Given the established role of *MGMT* methylation status for prognosis, we evaluated whether imaging-based HRV could provide complementary value in predicting survival. Information about MGMT methylation status was obtained for 61 patients in the TCIA cohort from a previous study [2]. Finally, we evaluated the relationships between

HRV and the mutation status of 9 genes that are known to have important functions in GBM, including *TP53*, *RB1*, *IDH1*, *PIK3R1*, *PTEN*, *PDGFRA*, *NF1*, *EGFR*, and *PIK3CA* [2].

Statistical analysis

Survival prediction performances of the HRV were assessed by the concordance index (CI) [37] and Cox regression analysis. Survival differences among two or more patient groups were compared by the log-rank test as well as Kaplan-Meier analysis. One-way ANOVA was performed to analyze the correlation between a continuous variable (e.g., the HRV) and a nominal variable (e.g., molecular subtype). P values smaller than 0.05 were considered significant. All statistical analyses were done in the open-source statistical computing environment R.

Results

HRV predicted overall survival, independent of clinical factors and other imaging metrics in the overall cohort

In the discovery cohort, we determined the thresholds for defining the HRV to be t_1=1.429, t_2=1.321 for the normalized T1-c and ADC intensities, respectively (Fig. 2). Using this definition, HRV achieved a CI score of 0.642, and was significantly correlated with OS on univariate Cox regression analysis (P<0.001). HRV remained as a significant predictor of OS (P<0.001) when adjusted for clinical variables including age, Karnofsky performance status (KPS), eloquent brain involvement (EBI, encoded as a binary variable), and conventional imaging metrics including ETV and minimum ADC (Table 2). An optimal cutoff of 5.12 cm^3 for HRV stratified the discovery cohort in terms of OS (Fig. 3A, log-rank P=0.009, hazard ratio=2.413).

In the validation cohort, HRV achieved a similar CI of 0.653, and was again significantly correlated with OS (*P*=0.038). Further, using the same cutoff derived from the discovery cohort, we stratified the validation cohort into short and long-survival groups, with a median survival of 9.3 months 13.7 months (Fig. 3B, log-rank *P*=0.009, hazard ratio=2.718). However, in the validation cohort alone, HRV was not significant (P=0.20) in multivariate analysis, nor was any of the other analyzed risk factors (P=0.13-0.74), possibly due to the smaller size of this cohort. Therefore, in order to increase the statistical power, we combined the discovery and validation cohorts together and performed multivariate analysis on this overall cohort again. The result showed that HRV was indeed a significant OS predictor in the overall cohort, independent of clinical factors and other imaging metrics.

Reproducibility of tumor segmentation and definition of HRV

The two independently delineated tumor volumes showed mostly high inter-observer agreement, with the Dice indices ranging from 0.623 to 0.985 (median: 0.948). Importantly, the HRVs computed from the two tumor segmentations were highly concordant (Supplemental Material Fig. S1), with an intra-class correlation of 0.994 (95% confidence interval = [0.990, 0.994], *P*<1E-16).

HRV stratified patients within the proneural molecular subtype

One-way ANOVA showed that HRV was not significantly correlated with the four GBM subtypes (*P*=0.1124). However, we found that the tumors of the proneural subtype tended to have the smallest HRV, which was confirmed by pair-wise comparison with the other three subtypes (Fig. 4, *P*=0.014-0.038). Furthermore, HRV was significantly associated with OS within the proneural group (CI=0.696, *P*=0.003). Using the median (2.29 cm^3) as a cutoff, HRV stratified patients with proneural tumors into short and long-survival groups, with a median survival of 6.4 months versus 12.3 months (Fig. 5A, log-rank *P*=0.040, hazard ratio=2.787). HRV did not stratify patients among other molecular subtypes.

HRV provided complementary information to MGMT methylation

HRV was not correlated with MGMT methylation status (*P*=0.1746). Survival stratification based on MGMT methylation status alone trended toward significance (log-rank *P*=0.072, hazard ratio=1.762). However, by combining methylation status and HRV (using median as the cutoff), we observed significantly different OS among the four groups (Fig. 5B, log-rank *P*=0.011), i.e., methylated MGMT and low HRV (n = 7), methylated MGMT and high HRV (n = 6), unmethylated MGMT and low HRV (n = 21), and unmethylated MGMT and high HRV (n = 28). Of note, patients with unmethylated MGMT and high HRV had much shorter survival compared with the others (median survival: 9.3 versus 18.4 months, log-rank *P*=0.002).

Higher HRV was associated with NF1 and PIK3CA mutation

HRV was significantly different between mutated and wide-type groups for *NF1* (*P*=0.049) and *PIK3CA* (*P*=0.028). Tumors with mutation in either *NF1* or *PIK3CA* had higher HRV than those of the wild type (Supplemental Material Fig. S2).

Discussion

In this study, we identified high-risk intratumoral subregions by using a data-driven approach and defined a volume-based imaging marker by integrating multi-parametric MR images of GBM. We found that HRV was prognostic for overall survival in two independent multi-institutional cohorts, and remained a significant predictor after adjusting for clinical factors and other imaging metrics. The predictive accuracy of HRV was higher than gross tumor volume, suggesting that analysis of intratumoral subregions may afford more reliable indicators of tumor burden compared with the whole tumor. HRV was also superior to minimum ADC, which points to the benefits of volume-based metrics versus conventional single-voxel approaches.

We used the kernel density estimation and mode approach under two scenarios: to obtain a patient-specific background voxel value for image normalization, and to find a population-level cutoff for defining the high-risk volume. In both scenarios, this approach has important advantages in that the mode value is a more robust statistic of the pooled distribution compared with other commonly used summary statistics (e.g., mean, median, or quantile values) [3; 6; 13], which may be sensitive to variations in tumor segmentation [38; 39]. Compared with previous approaches that require manual selection of a region of interest for image normalization [33], ours is fully automated and more robust.

Recent studies have used a quantitative radiomic approach to obtain comprehensive tumor phenotypes such as shape and texture. While further validation is warranted, this approach has showed promising results in identifying prognostic imaging markers in GBM and appears to provide additional information beyond simple volume-based imaging metrics [20; 23; 40; 41]. Previously this approach has mostly been applied to the primary tumor to extract whole-tumor aggregate characteristics. It would be interesting to apply radiomics to the high-risk intratumoral subregions extracted in this work to derive further improvement in prognostic value [19].

Our radiogenomic analysis revealed that the proposed imaging marker (HRV) was associated with several important molecular features of GBM. We showed that HRV was associated with overall survival and further stratified the proneural group. Compared with other molecular subtypes, the proneural group tended to harbor smaller HRV, which was correlated with longer survival. This is consistent with previous studies showing that the proneural molecular subtype had a better prognosis than others [2].

We showed that higher HRV was associated with mutations in NF1 and PIK3CA, which are key genetic events driving the progression of GBM [2]. *NF1* is a tumor-suppressor gene and frequently inactivated in GBM [2; 42]. It has been shown that NF1 mutation is highly enriched in the mesenchymal molecular subtype, a known aggressive GBM subtype with poor outcomes [2]. The *PI3K* signaling pathway is frequently dysregulated in GBM, and plays a critical role in proliferation, cellular metabolism, and apoptosis [43]. Therapeutic agents inhibiting PI3K activity are under active development and have the potential for improvement in clinical outcome for GBM [44]. *IDH1* mutation has been shown to be an independent prognostic factor in patients diagnosed with glioma including GBM [45], but appeared to be not associated with HRV in our study (Fig. S2), suggesting that they may be driven by differing biological processes.

Importantly, we showed that HRV provided complementary information to *MGMT* methylation status for survival prediction. Patients with unmethylated *MGMT* and high HRV had much shorter survival compared with other), while MGMT methylation status alone was not prognostic within our study cohort. This is consistent with a recent study [6] showing worse prognosis for patients with unmethylated *MGMT* and lower mean ADC. Taken together, these data support that the imaging-based HRV recapitulates tumor biology of GBM and potentially could provide additional prognostic information beyond genomic analysis.

Limitations of our study include the retrospective design and relatively small validation cohorts. The image data came from multiple institutions and were acquired with different imaging protocols and parameters, which might have influenced the image quantification. Nevertheless, we used careful image standardization techniques and robust image analysis to minimize the potential biases. Our findings warrant further validation in larger prospective cohorts. Intra-tumor genetic heterogeneity in GBM [46; 47] may confound the radiogenomic analyses. Because imaging has the unique capability of sampling the entire tumor and surrounding tissue, it would be intriguing to prospectively test the idea that combines imageguided stereotactic biopsy [48; 49] and the proposed method to identify high-risk intratumoral subregions, which might increase the likelihood of detecting the most aggressive part of a tumor.

Future studies would benefit from the incorporation of additional imaging modalities such as T2-weighted FLAIR and perfusion-weighted imaging for more comprehensive characterization of GBM such as surrounding edema/invasion [26] and blood volume/flow [3]. We also plan to test the ability of HRV to evaluate treatment response of GBM, in particular, to distinguish progression from pseudo-progression after chemoradiation therapy [50; 51].

In conclusion, volume of the high-risk intratumoral subregion on multi-parametric MRI predicts overall survival in GBM patients, and may provide complementary value to genomic information. We envision that the same approach could be applied to identify clinically and biologically relevant imaging markers in other cancer types.

Compliance with ethical standards:

Guarantor:

The scientific guarantor of this publication is Dr. Ruijiang Li.

Conflict of interest:

The authors of this manuscript declare no relationships with any companies, whose products or services may be related to the subject matter of the article.

Funding:

This research was partially funded by the NIH (grant number: R01 CA193730), and partially supported by the Global Institution for Collaborative Research and Education (GI-CoRE), Hokkaido University, founded by the Ministry of Education, Culture, Sports, Science and

Technology MEXT, Japan. Part of the data used in this research was obtained from The Cancer Imaging Archive (TCIA) sponsored by the Cancer Imaging Program, DCTD/NCI/NIH.

Statistics and biometry:

One of the authors has significant statistical expertise.

Ethical approval:

Institutional Review Board approval was obtained.

Informed consent:

Written informed consent was waived by the Institutional Review Board.

Methodology:

- retrospective
- diagnostic or prognostic study
- multicenter study

References

1 Ostrom QT, Gittleman H, Fulop J et al (2015) CBTRUS Statistical Report: Primary Brain and Central Nervous System Tumors Diagnosed in the United States in 2008-2012. Neuro Oncol 17 Suppl 4:iv1-iv62

2 Verhaak RG, Hoadley KA, Purdom E et al (2010) Integrated genomic analysis identifies clinically relevant subtypes of glioblastoma characterized by abnormalities in PDGFRA, IDH1, EGFR, and NF1. Cancer Cell 17:98-110

3 Jain R, Poisson L, Narang J et al (2013) Genomic mapping and survival prediction in glioblastoma: molecular subclassification strengthened by hemodynamic imaging biomarkers. Radiology 267:212-220

4 Burth S, Kickingereder P, Eidel O et al (2016) Clinical parameters outweigh diffusion- and perfusion-derived MRI parameters in predicting survival in newly diagnosed glioblastoma. Neuro Oncol. 10.1093/neuonc/now122

5 Schmainda KM, Zhang Z, Prah M et al (2015) Dynamic susceptibility contrast MRI measures of relative cerebral blood volume as a prognostic marker for overall survival in recurrent glioblastoma: results from the ACRIN 6677/RTOG 0625 multicenter trial. Neuro Oncol 17:1148-1156

6 Choi YS, Ahn SS, Kim DW et al (2016) Incremental Prognostic Value of ADC Histogram Analysis over MGMT Promoter Methylation Status in Patients with Glioblastoma. Radiology. 10.1148/radiol.2016151913:151913

7 Gupta A, Prager A, Young RJ, Shi W, Omuro AM, Graber JJ (2013) Diffusion-weighted MR imaging and MGMT methylation status in glioblastoma: a reappraisal of the role of preoperative quantitative ADC measurements. AJNR Am J Neuroradiol 34:E10-11

8 Moon WJ, Choi JW, Roh HG, Lim SD, Koh YC (2012) Imaging parameters of high grade gliomas in relation to the MGMT promoter methylation status: the CT, diffusion tensor imaging, and perfusion MR imaging. Neuroradiology 54:555-563

9 Pope WB, Lai A, Mehta R et al (2011) Apparent Diffusion Coefficient Histogram Analysis Stratifies Progression-Free Survival in Newly Diagnosed Bevacizumab-Treated Glioblastoma. American Journal of Neuroradiology 32:882-889

10 Romano A, Calabria LF, Tavanti F et al (2013) Apparent diffusion coefficient obtained by magnetic resonance imaging as a prognostic marker in glioblastomas: correlation with MGMT promoter methylation status. European Radiology 23:513-520

11 Saksena S, Jain R, Narang J et al (2010) Predicting Survival in Glioblastomas Using Diffusion Tensor Imaging Metrics. Journal of Magnetic Resonance Imaging 32:788-795

12 Sunwoo L, Choi SH, Park CK et al (2013) Correlation of apparent diffusion coefficient values measured by diffusion MRI and MGMT promoter methylation semiquantitatively analyzed with MS-MLPA in patients with glioblastoma multiforme. Journal of Magnetic Resonance Imaging 37:351-358

13 Higano S, Yun X, Kumabe T et al (2006) Malignant astrocytic tumors: Clinical importance of apparent diffusion coefficient in prediction of grade and prognosis. Radiology 241:839-846

14 Wangaryattawanich P, Hatami M, Wang J et al (2015) Multicenter imaging outcomes study of The Cancer Genome Atlas glioblastoma patient cohort: imaging predictors of overall and progression-free survival. Neuro Oncol 17:1525-1537

15 Ellingson BM, Harris RJ, Woodworth DC et al (2016) Baseline pretreatment contrast enhancing tumor volume including central necrosis is a prognostic factor in recurrent glioblastoma: evidence from single- and multicenter trials. Neuro Oncol. 10.1093/neuonc/now187

16 Zhang M, Gulotta B, Thomas A et al (2016) Large-volume low apparent diffusion coefficient lesions predict poor survival in bevacizumab-treated glioblastoma patients. Neuro Oncol 18:735-743

17 Gatenby RA, Grove O, Gillies RJ (2013) Quantitative imaging in cancer evolution and ecology. Radiology 269:8-15

18 Ling CC, Humm J, Larson S et al (2000) Towards multidimensional radiotherapy (MD-CRT): biological imaging and biological conformality. Int J Radiat Oncol Biol Phys 47:551-560

19 Cui Y, Tha KK, Terasaka S et al (2016) Prognostic Imaging Biomarkers in Glioblastoma: Development and Independent Validation on the Basis of Multiregion and Quantitative Analysis of MR Images. Radiology 278:546-553

20 Chang K, Zhang B, Guo X et al (2016) Multimodal imaging patterns predict survival in recurrent glioblastoma patients treated with bevacizumab. Neuro Oncol. 10.1093/neuonc/now086

21 Chenevert TL, Malyarenko DI, Newitt D et al (2014) Errors in Quantitative Image Analysis due to Platform-Dependent Image Scaling (vol 7, pg 65, 2014). Translational Oncology 7:523-523

22 Ellingson BM, Lai A, Nguyen HN, Nghiemphu PL, Pope WB, Cloughesy TF (2015) Quantification of Nonenhancing Tumor Burden in Gliomas Using Effective T-2 Maps Derived from Dual-Echo Turbo Spin-Echo MRI. Clinical Cancer Research 21:4373-4383

23 Gevaert O, Mitchell LA, Achrol AS et al (2014) Glioblastoma multiforme: exploratory radiogenomic analysis by using quantitative image features. Radiology 273:168-174

24 Gutman DA, Cooper LA, Hwang SN et al (2013) MR imaging predictors of molecular profile and survival: multi-institutional study of the TCGA glioblastoma data set. Radiology 267:560-569

25 Jamshidi N, Diehn M, Bredel M, Kuo MD (2014) Illuminating Radiogenomic Characteristics of Glioblastoma Multiforme through Integration of MR Imaging, Messenger RNA Expression, and DNA Copy Number Variation. Radiology 270:212-222

26 Zinn PO, Mahajan B, Sathyan P et al (2011) Radiogenomic mapping of edema/cellular invasion MRI-phenotypes in glioblastoma multiforme. PLoS One 6:e25451

27 Klein S, Staring M, Murphy K, Viergever MA, Pluim JPW (2010) elastix: A Toolbox for Intensity-Based Medical Image Registration. Ieee Transactions on Medical Imaging 29:196-205

28 Mohammadi S, Moller HE, Kugel H, Muller DK, Deppe M (2010) Correcting eddy current and motion effects by affine whole-brain registrations: evaluation of three-dimensional distortions and comparison with slicewise correction. Magn Reson Med 64:1047-1056

29 Botev ZI, Grotowski JF, Kroese DP (2010) Kernel Density Estimation Via Diffusion. Annals of Statistics 38:2916-2957

30 Ogura A, Tamura T, Ozaki M et al (2015) Apparent Diffusion Coefficient Value Is Not Dependent on Magnetic Resonance Systems and Field Strength Under Fixed Imaging Parameters in Brain. J Comput Assist Tomogr 39:760-765

31 Lemkaddem A, Daducci A, Vulliemoz S et al (2012) A multi-center study: intra-scan and inter-scan variability of diffusion spectrum imaging. Neuroimage 62:87-94

32 Grech-Sollars M, Hales PW, Miyazaki K et al (2015) Multi-centre reproducibility of diffusion MRI parameters for clinical sequences in the brain. NMR Biomed 28:468-485

33 Barajas RF, Hodgson JG, Chang JS et al (2010) Glioblastoma Multiforme Regional Genetic and Cellular Expression Patterns: Influence on Anatomic and Physiologic MR Imaging. Radiology 254:564-576

34 McAuliffe MJ, Lalonde FM, McGarry D, Gandler W, Csaky K, Trus BL (2001) Medical Image Processing, Analysis & Visualization in clinical research. Fourteenth Ieee Symposium on Computer-Based Medical Systems, Proceedings:381-386

35 Goldman M, Craft B, Swatloski T et al (2015) The UCSC Cancer Genomics Browser: update 2015. Nucleic Acids Res 43:D812-817

36 Zhu J, Sanborn JZ, Benz S et al (2009) The UCSC Cancer Genomics Browser. Nat Methods 6:239-240

37 Harrell FE (2001) Regression modeling strategies : with applications to linear models, logistic regression, and survival analysis. Springer, New York ; London

38 Leijenaar RT, Carvalho S, Velazquez ER et al (2013) Stability of FDG-PET Radiomics features: an integrated analysis of test-retest and inter-observer variability. Acta Oncol 52:1391-1397

39 Parmar C, Rios Velazquez E, Leijenaar R et al (2014) Robust Radiomics feature quantification using semiautomatic volumetric segmentation. PLoS One 9:e102107

40 Macyszyn L, Akbari H, Pisapia JM et al (2016) Imaging patterns predict patient survival and molecular subtype in glioblastoma via machine learning techniques. Neuro Oncol 18:417-425

41 Kickingereder P, Bonekamp D, Nowosielski M et al (2016) Radiogenomics of Glioblastoma: Machine Learning-based Classification of Molecular Characteristics by Using Multiparametric and Multiregional MR Imaging Features. Radiology. 10.1148/radiol.2016161382:161382

42 Cancer Genome Atlas Research N (2008) Comprehensive genomic characterization defines human glioblastoma genes and core pathways. Nature 455:1061-1068

43 Engelman JA (2009) Targeting PI3K signalling in cancer: opportunities, challenges and limitations. Nat Rev Cancer 9:550-562

44 Wen PY, Lee EQ, Reardon DA, Ligon KL, Alfred Yung WK (2012) Current clinical development of PI3K pathway inhibitors in glioblastoma. Neuro Oncol 14:819-829

45 Sanson M, Marie Y, Paris S et al (2009) Isocitrate dehydrogenase 1 codon 132 mutation is an important prognostic biomarker in gliomas. J Clin Oncol 27:4150-4154

46 Patel AP, Tirosh I, Trombetta JJ et al (2014) Single-cell RNA-seq highlights intratumoral heterogeneity in primary glioblastoma. Science 344:1396-1401

47 Sottoriva A, Spiteri I, Piccirillo SG et al (2013) Intratumor heterogeneity in human glioblastoma reflects cancer evolutionary dynamics. Proc Natl Acad Sci U S A 110:4009-4014

48 Barajas RF, Jr., Phillips JJ, Parvataneni R et al (2012) Regional variation in histopathologic features of tumor specimens from treatment-naive glioblastoma correlates with anatomic and physiologic MR Imaging. Neuro Oncol 14:942-954

49 Hu LS, Ning S, Eschbacher JM et al (2016) Radiogenomics to characterize regional genetic heterogeneity in glioblastoma. Neuro Oncol. 10.1093/neuonc/now135

50 Chu HH, Choi SH, Ryoo I et al (2013) Differentiation of true progression from pseudoprogression in glioblastoma treated with radiation therapy and concomitant temozolomide: comparison study of standard and high-b-value diffusion-weighted imaging. Radiology 269:831-840

51 Park JE, Kim HS, Goh MJ, Kim SJ, Kim JH (2015) Pseudoprogression in Patients with Glioblastoma: Assessment by Using Volume-weighted Voxel-based Multiparametric Clustering of MR Imaging Data in an Independent Test Set. Radiology 275:792-802

Figure captions

Figure 1: Flow-chart of the proposed study design. The TCIA cohort was randomly split into the discovery cohort and a spin-off cohort which was further combined with an internal cohort to construct the validation cohort. The proposed imaging marker was developed on the discovery cohort and its performance for OS prediction was also evaluated on the validation cohort. The subtype, mutation, and methylation data associated with the TCIA cohort were used to correlate with the proposed imaging marker to show its biological relevance and complementarity to molecular-level information.

Figure 2: Diagram of the procedure of high-risk volume identification. In Step 1, the T1-c and ADC images for each patient were respectively normalized using the mode values of the intensity PDF estimates. In Step 2, the normalized intensities of the pixels within the segmented tumors (shaded in red) of all patients were pooled and two thresholds (t_1, t_2) were respectively obtained as the mode values of the pooled intensity PDF estimates. In Step 3, HRV for each patient was defined as the volume of the tumor satisfying T1-c > t_1 and ADC < t_2.

Figure 3: Kaplan-Meier survival estimates for the discovery (A) and the validation (B) cohorts using HRV.

Figure 4: Boxplot shows that HRV was the smallest in the proneural subtype among the four GBM molecular subtypes. The P-value is for one-way ANOVA.

Figure 5: Radiogenomic analysis of HRV. (A) Kaplan-Meier survival estimates for proneural patients using HRV. (A) Kaplan-Meier survival estimates based on both methylation status and HRV.

Table

Table 1: Demographic and clinical information of study population.

	Overall Cohort	TCIA Cohort	Local Cohort	Discovery Cohort	Validation Cohort
Number†	108 (23)	92 (15)	16 (7)	62 (9)	46 (14)
Age‡ (years)	58.1 ± 14.8	57.9 ± 14.5	58.9 ± 16.9	57.7 ± 14.1	58.5 ± 15.8
Karnofsky Performance Scale††	80 (60–100)*	80 (60–100)*	N/A	80 (60–100)*	80 (60–100)*
Overall Survival†† (days)	357 (16–1757)	362 (16–1757)	288 (37–713)	357 (16–1757)	426 (34–1561)
Gender					
Male	63	56	7	43	20
Female	45	36	9	19	26
Molecular Subtypes					
Classical	17	17	0	10	7
Proneural	24	24	0	16	8
Neural	21	21	0	14	7
Mesenchymal	26	26	0	18	8
Unknown	20	4	16	4	16
Methylation Status					
Methylated	12	12	0	6	6
Unmethylated	49	49	0	33	16
Unknown	47	31	16	23	24

Note. –Unless otherwise indicated, data are patient numbers.

† Data in parenthesis are censored patient numbers.

‡ Data are mean ± standard deviation

†† Data are median (range).

* Missing data were imputed with median value.

Table 2: Prognostic performances of high-risk volume in comparison with clinical and baseline indicators.

Cohort	Risk factor	Concordance Index	Univariate Analysis		Multivariate Analysis	
			P-Value	Hazard Ratio	*P*-Value	Hazard Ratio
Discovery	HRV	0.64 (0.45, 0.80)	3.9E-4***	1.63 (1.25, 2.14)	4.78E-3**	1.83 (1.20, 2.78)
	Age	0.64 (0.45, 0.80)	3.4E-3**	1.71 (1.20, 2.45)	2.15E-3**	1.77 (1.23, 2.56)
	KPS	0.37 (0.19, 0.59)	0.20	0.83 (0.63, 1.10)	0.73	0.95 (0.71, 1.27)
	ETV	0.60 (0.41, 0.76)	0.09	1.25 (0.96, 1.61)	0.98	1.01 (0.70, 1.43)
	EBI	0.52 (0.28, 0.76)	0.55	0.84 (0.48, 1.48)	0.28	0.71 (0.39, 1.31)
	Minimum ADC	0.43 (0.26, 0.62)	0.12	0.80 (0.61, 1.06)	0.94	1.01 (0.71, 1.44)
Validation	HRV	0.65 (0.42, 0.83)	0.04*	1.39 (1.01, 1.92)	0.20	1.97 (0.70, 5.56)
	Age	0.58 (0.35, 0.78)	0.23	1.32 (0.84, 2.09)	0.70	1.11 (0.66, 1.84)
	KPS	0.50 (0.25, 0.75)	0.38	0.86 (0.60, 1.21)	0.74	1.08 (0.69, 1.69)
	ETV	0.57 (0.34, 0.77)	0.20	1.23 (0.90, 1.68)	0.44	0.70 (0.28, 1.74)
	EBI	0.76 (0.43, 0.93)	0.02*	2.42 (1.16, 5.04)	0.13	2.06 (0.80, 5.30)
	Minimum ADC	0.53 (0.31, 0.74)	0.84	1.04 (0.70, 1.55)	0.47	1.21 (0.73, 2.00)
Discovery + Validation	HRV	0.64 (0.49, 0.77)	2.6E-4***	1.43 (1.18, 1.73)	0.03*	1.53 (1.04, 2.25)
	Age	0.61 (0.46, 0.74)	4.1E-3**	1.48 (1.13, 1.94)	4.8E-3**	1.50 (1.13, 1.99)
	KPS	0.41 (0.26, 0.58)	0.08	0.82 (0.66, 1.02)	0.23	0.87 (0.69, 1.09)
	ETV	0.59 (0.44, 0.73)	0.03	1.24 (1.02, 1.51)	0.72	0.94 (0.62, 1.35)
	EBI	0.61 (0.40, 0.78)	0.27	1.27 (0.83, 1.95)	0.57	0.87 (0.54, 1.41)
	Minimum ADC	0.46 (0.32, 0.61)	0.16	0.85 (0.68, 1.07)	0.60	0.93 (0.72, 1.21)

Note. –Unless otherwise indicated, data in parenthesis are 95% confidence intervals.

Abbreviations. –HRV: high-risk volume, KPS: Karnofsky performance status, ETV: enhancing tumor volume, ADC: apparent diffusion coefficient, EBI: eloquent brain involvement

* P<0.05

** P<0.005

*** P<0.0005

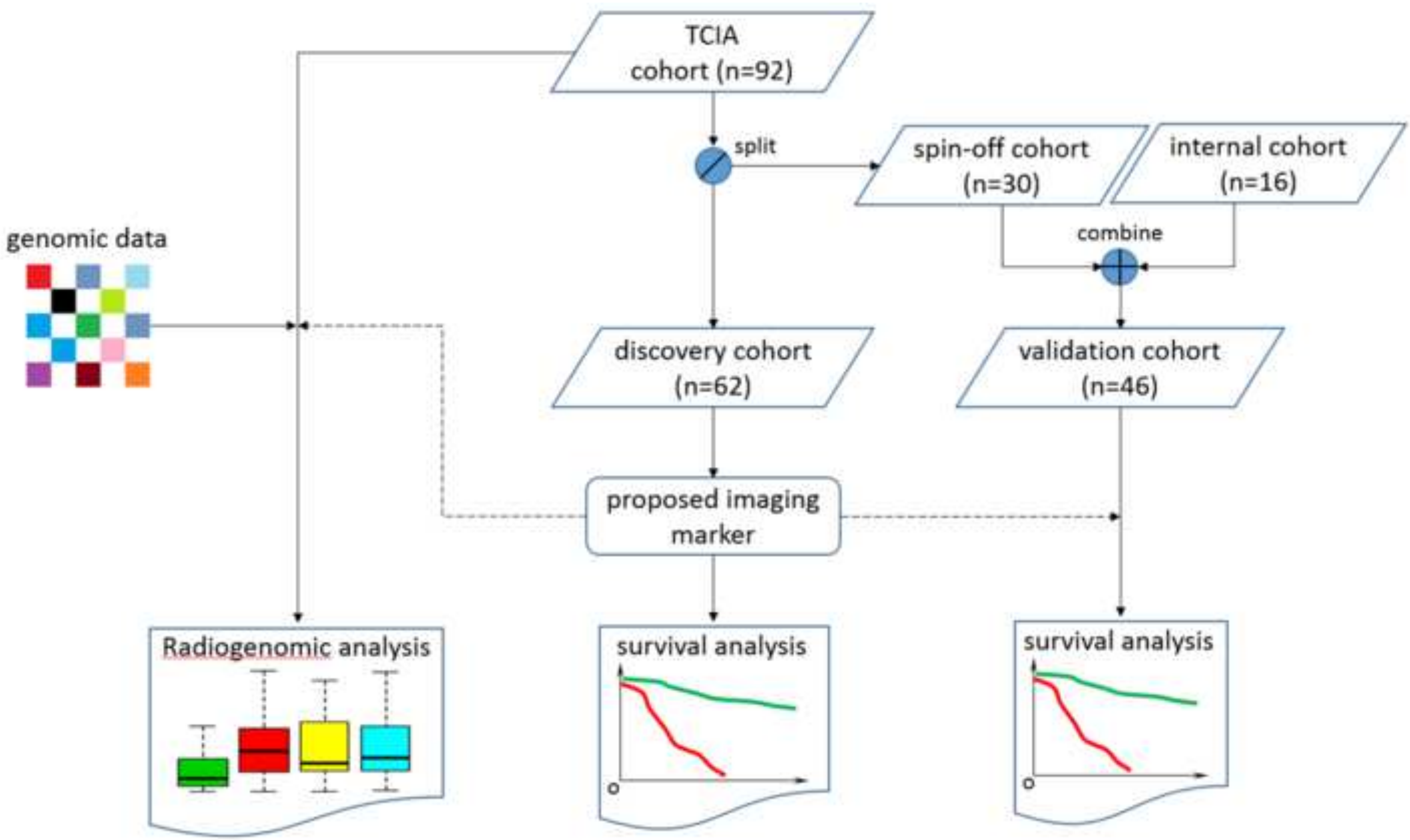
TCIA
cohort (n=92)
split
spin-off cohort
(n=30)
internal cohort
(n=16)
combine
genomic data
discovery cohort
(n=62)
validation cohort
(n=46)
proposed imaging
marker
Radiogenomic analysis
survival analysis
0
survival analysis
0

Fig2

Click here to download Figure Figure_2.tif

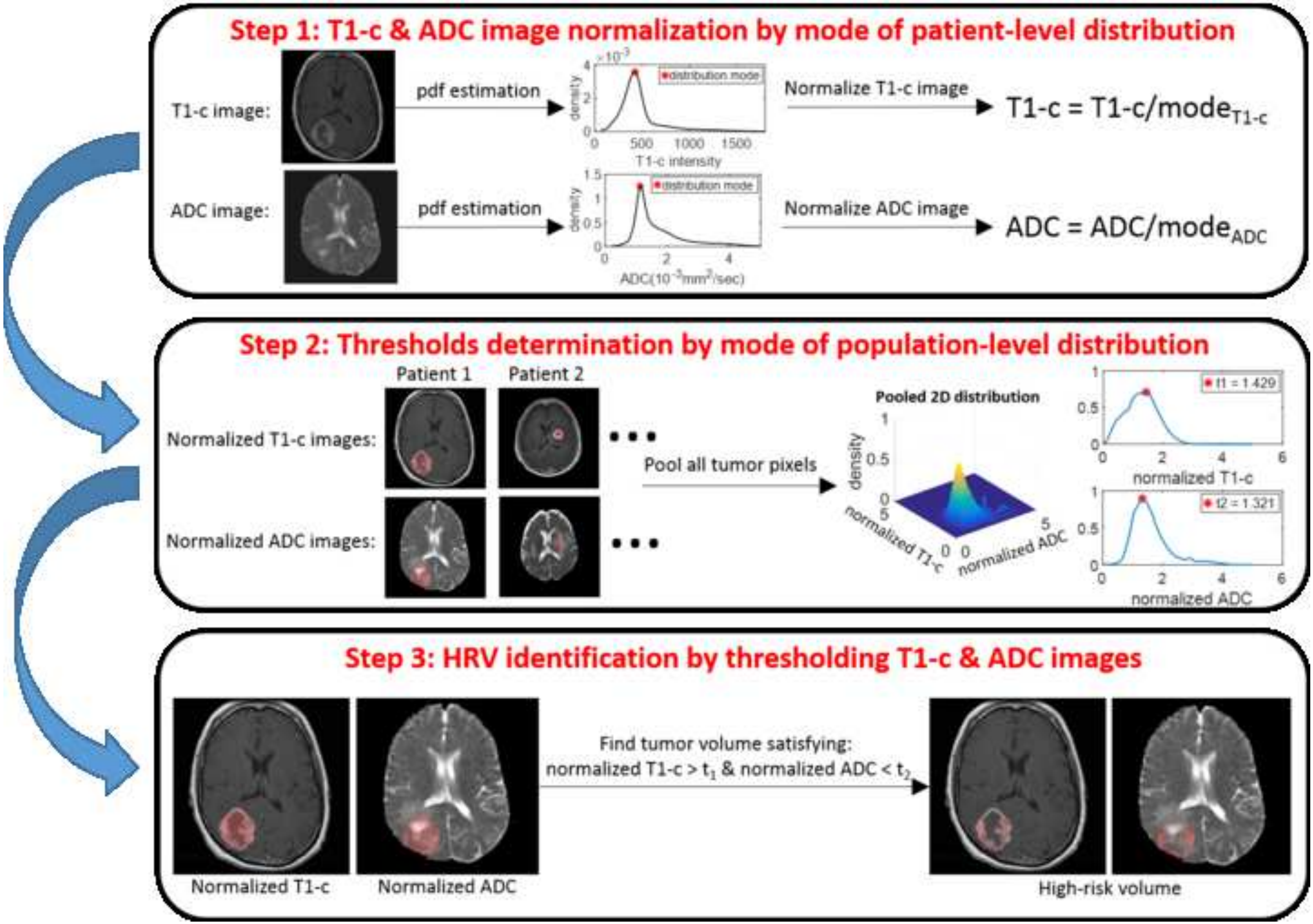

Fig3

Click here to download Figure Figure_3.tif

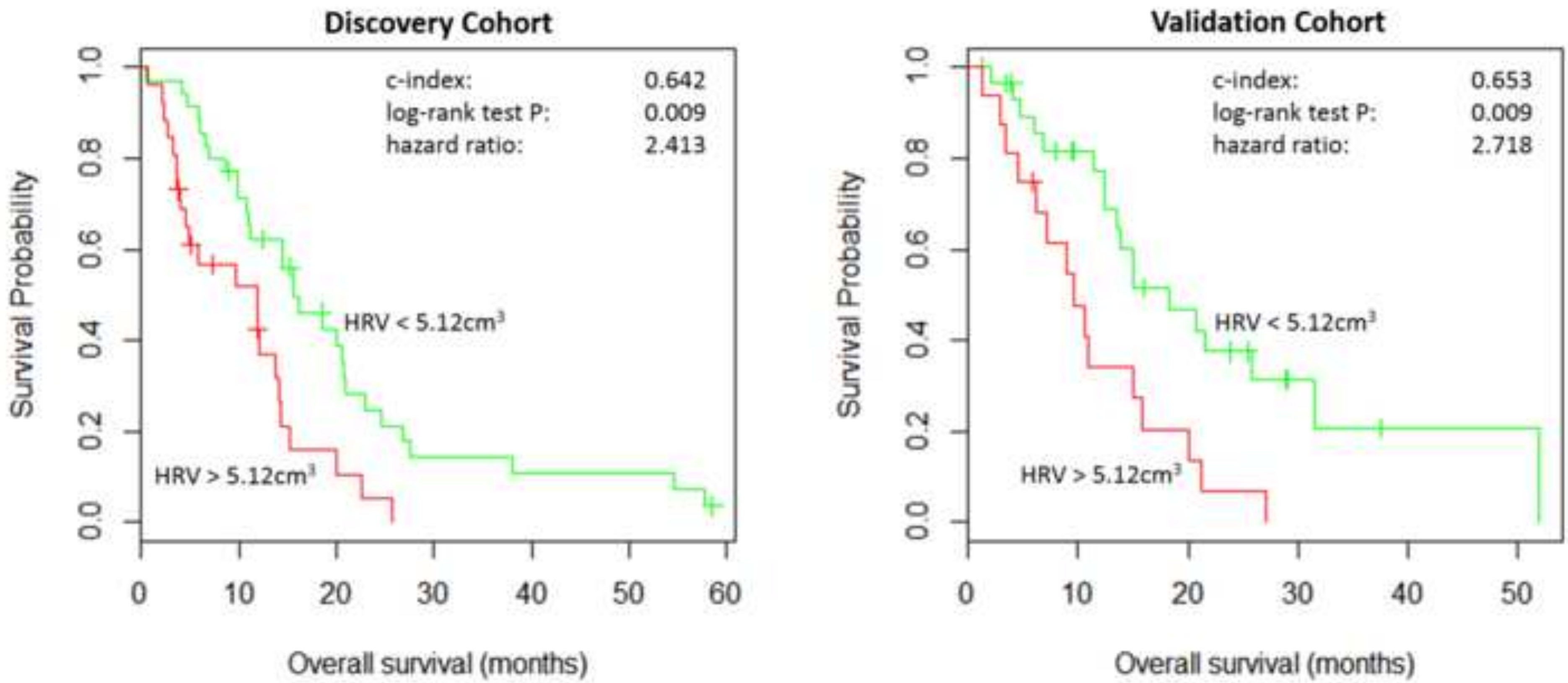

Fig4 Click here to download Figure Figure_4.tif

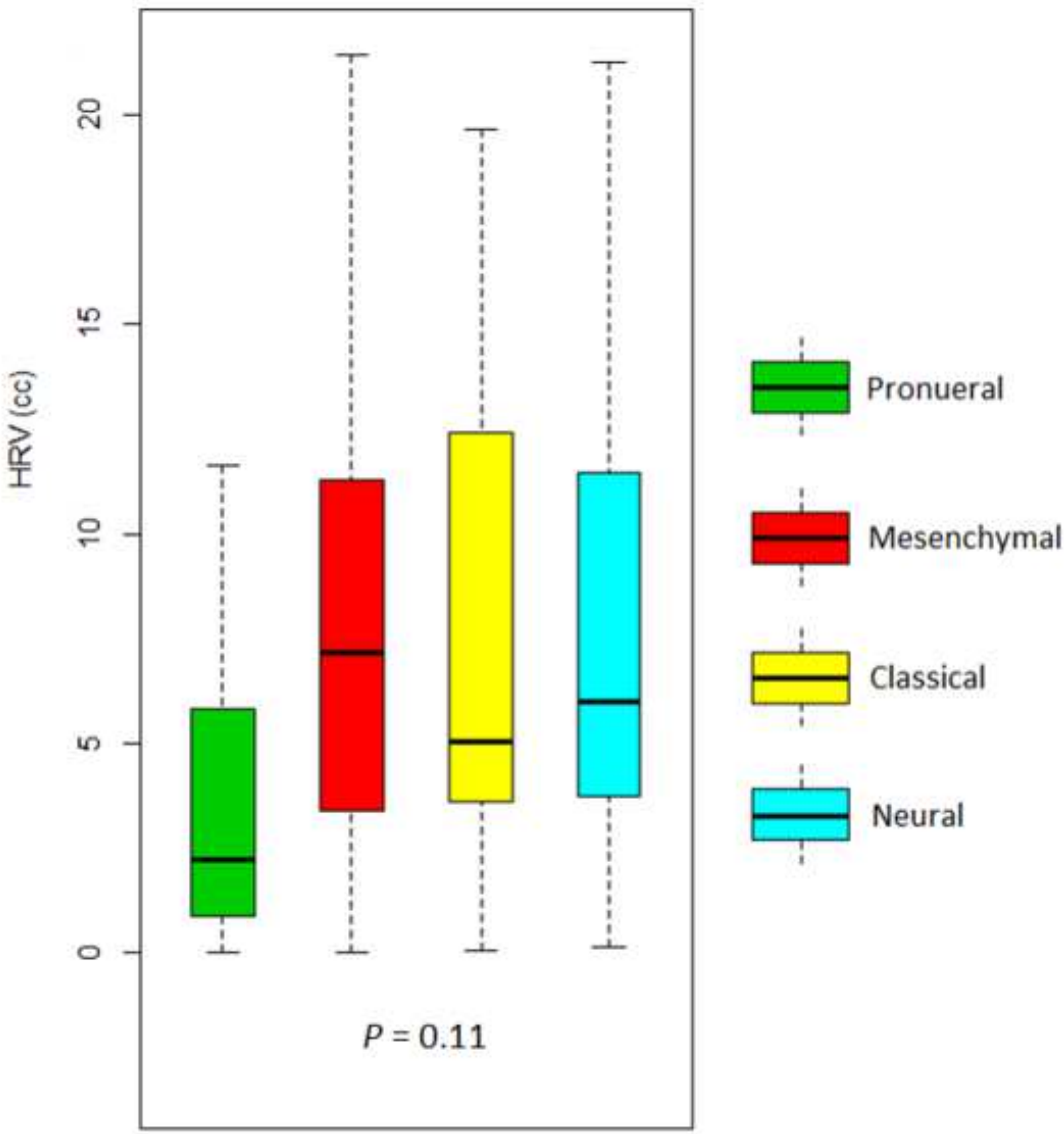

Fig5

Click here to download Figure Figure_5.tif